Thermodynamics and kinetics of the $Mg_{65}Cu_{25}Y_{10}$ bulk metallic glass forming liquid

R. Busch,[a] W. Liu, and W. L. Johnson
California Institute of Technology, W. M. Keck Laboratory of Engineering Materials, 138-78, Pasadena, California 91125

(Received 8 December 1997; accepted for publication 12 January 1998)

The thermodynamics and kinetics of the bulk metallic glass forming $Mg_{65}Cu_{25}Y_{10}$ liquid were investigated using differential scanning calorimetry and three-point beam bending. The experiments lead to the determination of the thermodynamic functions as well as the viscosity of the supercooled liquid. The viscosity shows a temperature dependence, which is consistent with that of a strong glass similar to Zr–Ti–Cu–Ni–Be bulk metallic glasses or sodium silicate glasses. This contrasts with more fragile conventional metallic glass formers or pure metals. The relatively weak temperature dependence of the thermodynamic functions of the supercooled liquid is related to these sluggish kinetics in the supercooled liquid. Entropy, viscosity, and kinetic glass transition are compared in the frameworks of the fragility concept and the Adam–Gibbs theory. Strong liquid behavior retards the formation of crystals kinetically and thermodynamically. © *1998 American Institute of Physics.* [S0021-8979(98)04408-9]

I. INTRODUCTION

During the past several years, new families of multicomponent glass forming alloys such as La–Al–Ni,[1] Zr–Ni–Al–Cu,[2] Mg–Cu–Y,[3] and Zr–Ti–Cu–Ni–Be[4] have been discovered, which exhibit very good glass forming ability. These bulk metallic glass (BMG) formers show a high thermal stability of their supercooled liquid when heated above the glass transition temperature. This allows for detailed studies of the thermophysical properties of metallic melts in the deeply supercooled (undercooled) state. The thermophysical properties include specific heat capacity, viscosity, diffusion, surface tension, and thermal expansion coefficient. For the particular Zr–Ti–Cu–Ni–Be system, some thermophysical properties such as heat capacity,[5] viscosity,[6] diffusion,[7] and emissivity have been measured far into the supercooled region.[8]

In this article, we focus on thermodynamics and kinetics of the $Mg_{65}Cu_{25}Y_{10}$ alloy. This material is the best glass former of a family of Mg-based alloys that are interesting because of their high strength to weight ratio. The tensile fracture strength of the amorphous alloy is about 800 Mpa and thus about twice as large as for conventional Mg-based crystalline alloys. Fully amorphous rods of the particular $Mg_{65}Cu_{25}Y_{10}$ alloy can be prepared up to a thickness of 7 mm by high-pressure die casting.[3] The alloy has a low eutectic melting point of 730 K and a large supercooled liquid region when heated above the glass transition. Therefore it is possible to obtain very reliable thermodynamic data with one single differential scanning calorimeter (DSC). Viscosity measurements were performed in a thermal mechanical analyzer (TMA). The set of thermodynamic and kinetic data of the supercooled liquid will be compared and discussed especially in the framework of the fragility concept.

[a]Electronic mail: busch@hyperfine.caltech.edu

II. EXPERIMENTAL METHODS

$Mg_{65}Cu_{25}Y_{10}$ ingots were prepared from a mixture of the elements of purity ranging from 99.9% to 99.999% by induction melting on a water-cooled silver boat under a Ti-gettered argon atmosphere. They were further processed by casting into copper molds under inert gas atmosphere to form amorphous strips with a thickness of 1 mm. DSC measurements were performed in a Perkin-Elmer DSC7. The sample weights ranged from 4 to 50 mg. The samples were first heated up above the glass transition temperature to 443 K with a rate of 0.33 K/s and cooled with a rate of 3.3 K/s back to ambient temperature to ensure the same thermal history for all specimens. The calorimeter was recalibrated for each heating rate using the melting transition of indium and zinc standards in order to account for the temperature shift on changing heat rates. A second run with each specimen was directly carried out after the first cycle without changing the conditions of the measurement to construct a baseline.

The absolute values of the specific heat capacity of the amorphous alloys up to 403 K, the crystallized samples up to 730 K (melting point), and liquid from the melting point to 843 K were determined in reference to the specific heat capacity of a sapphire standard. The sample was first heated to a certain temperature with a constant rate of 0.33 K/s and then held isothermally for 180 s. This resulted in a step of the heat flux dQ/dt

$$\frac{dQ}{dt}=\left(\frac{\partial Q}{\partial t}\right)_{\dot{T}\neq 0}-\left(\frac{\partial Q}{\partial t}\right)_{\dot{T}=0}=C\cdot\frac{dT}{dt}. \tag{1}$$

The term $(\partial Q/\partial t)_{\dot{T}\neq 0}$ corresponds to the power, which is necessary to heat the sample and the container with an overall heat capacity C and hold it at a certain temperature. $(\partial Q/\partial t)_{\dot{T}=0}$ is the power, which is needed to keep the temperature just constant. To determine the absolute specific heat capacity of the sample, the heat capacity of the empty

sample container and of a sapphire standard was measured as well. The specific heat capacity of the sample was then calculated by the following formula:

$$c_p(T)_{\text{sample}} = \frac{\dot{Q}_{\text{sample}} - \dot{Q}_{\text{pan}}}{\dot{Q}_{\text{sapphire}} - \dot{Q}_{\text{pan}}} \cdot \frac{m_{\text{sapphire}} \cdot \mu_{\text{sample}}}{m_{\text{sample}} \cdot \mu_{\text{sapphire}}} \cdot c_p(T)_{\text{sapphire}}, \quad (2)$$

where m_i is the mass, μ_i the mole mass, and $c_p(T)_{\text{sapphire}}$ the specific heat capacity of sapphire. This procedure was done every 10 K. The samples were contained in molybdenum pans and scanned under argon atmosphere. No reaction between the container and the material was observed when the sample was melted in the molybdenum pan.

Three-point beam bending was used to measure viscosity. A load was applied to the center of a beam of uniform cross section supported on both ends. By measuring the deflection of the center of the beam with time, the viscosity can be derived. Viscosities in the range between 10^8 and 10^{15} poise were measured by this method.

The viscosity in Pa s can be found using the equation[9–11]

$$\eta = \frac{gL^3}{144 I_c} v \left(M + \frac{5\rho AL}{8} \right), \quad (3)$$

where g is the gravitational constant (9.8 m/s^2), I_c the cross-section moment of inertia (m^4), v the midpoint deflection rate (m/s), M the applied load (kg), ρ the density of the glass (kg/m^3), A the cross-sectional area (m^2), and L the support span (for out apparatus, $L = 5.08 \times 10^{-3}$ m).

The experimental apparatus was a Perkin-Elmer TMA 7. Beam samples of $Mg_{65}Cu_{25}Y_{10}$ with different rectangular cross sections were cut from 1 mm thick amorphous strips obtained by mold casting. The typical length of the beams was 8 mm and a typical cross section was 1×0.5 mm^2. Samples were heated from room temperature to the assigned temperature of the measurement with a heating rate of 0.833 K/s and then isothermally annealed at that temperature for different times from 30 to 5000 min, monitoring the viscosity. The applied force varied between 20 and 1000 mN depending on the expected viscosity at a given temperature.

III. RESULTS

A. Thermodynamics

The glass transition, crystallization, and the melting behavior of $Mg_{65}Cu_{25}Y_{10}$ alloy were measured in DSC scans with various heating rates. Figure 1 shows a typical DSC trace scanned with a heating rate of 0.33 K/s. It starts with an endothermic heat effect due to the glass transition followed by two exothermic peaks corresponding to two steps of crystallization. The primary crystallization begins at about 468 K. It corresponds to the transformation from the supercooled liquid into a mixture of nanocrystalline Mg_2Cu and a supercooled liquid matrix.[12] The sample starts to melt at the eutectic temperature 730 K followed by complete melting at 739 K. The scan shows a relatively sharp single endothermic melting peak that does not split into two peaks even for the smallest applied heating rate of 8.33×10^{-3} K/s. For this small heating rate the melting interval is not wider than 3 K. This indicates that the $Mg_{65}Cu_{25}Y_{10}$ alloy consists of a ternary Mg–Cu–Y eutectic composition.

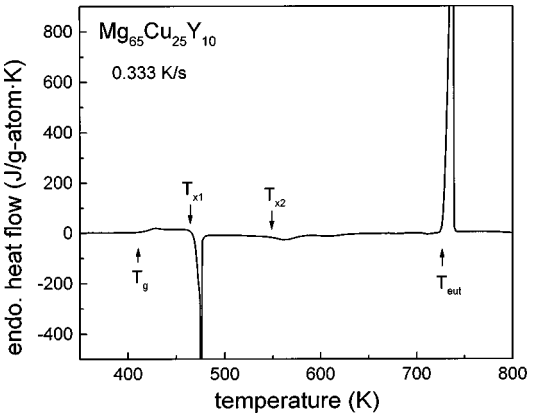

FIG. 1. DSC scan of an amorphous $Mg_{65}Cu_{25}Y_{10}$ sample alloy at a heating rate of 0.333 K/s. It shows the onset of the glass transition, T_g, two pronounced exothermal crystallization events T_{x1} and T_{x2}, as well as the endothermic melting at the eutectic temperature, T_{eut}.

The measured heat of fusion is found to be 8.65 kJ/g atom. The total heat of crystallization from the supercooled liquid state into the crystalline mixture depends on the used heating rate.[5] For a rate of 0.33 K/s it is 5.40 kJ/g atom.

The difference between heat of fusion and heat of crystallization reflects a finite specific heat capacity difference between supercooled liquid and crystal. Figure 2 shows measured specific heat capacities of the equilibrium liquid, the supercooled liquid, the amorphous state, and the crystal, as they are obtained in reference to sapphire. According to Kubaschewski *et al.*,[13] the temperature dependence of the specific heat capacity, c_p, of the undercooled liquid far above Debye temperature can be expressed as

$$c_p(T) = 3R + a \cdot T + b \cdot T^{-2}, \quad (4)$$

where $R = 8.314$ J/g atom$\cdot K$. The specific heat capacity of the crystal is described with the equation

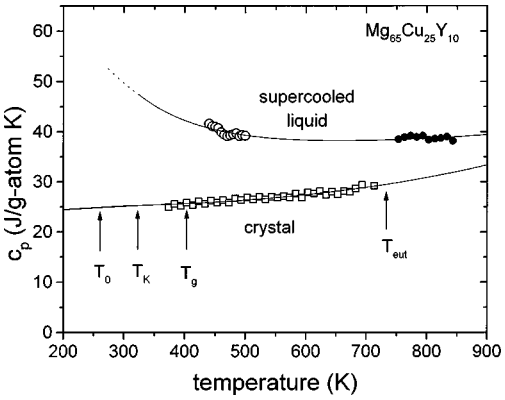

FIG. 2. Specific heat capacity of the equilibrium liquid (●), supercooled liquid (○), the amorphous alloy (△), and the crystalline mixture (□). The data of the liquid and the crystalline state were measured in steps in reference to sapphire. The data in the supercooled liquid were measured with constant heating rate. The straight lines represent the fits to Eqs. (4) and (5). The glass transition temperature T_g (onset with a rate of 0.0167 K/s, the Kauzmann temperature, T_K, and the VFT temperature T_0 are marked.

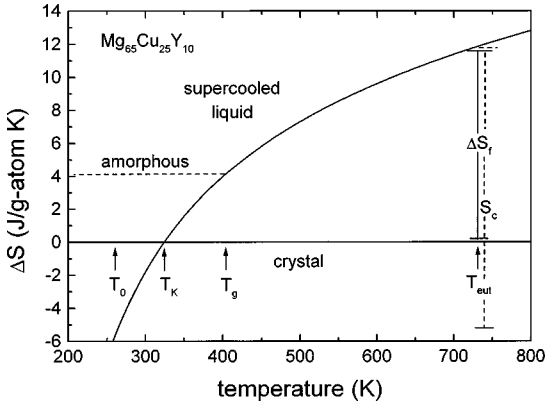

FIG. 3. Entropy of the undercooled liquid with respect to the crystal, including the entropy of fusion, ΔS_f, the glass transition temperature T_g (onset with a rate of 0.0167 K/s), the Kauzmann temperature T_K, and the VFT temperature T_0. The configurational entropy change S_c that has to be assumed when fitting the viscosity with Eqs. (8) and (9) is also shown.

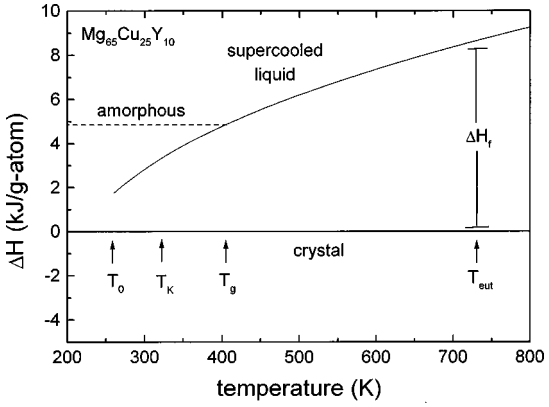

FIG. 4. Enthalpy of the undercooled liquid with respect to the crystal as a function of temperature.

$$c_p(T) = 3R + c \cdot T + d \cdot T^2. \tag{5}$$

The constants are found to be $a = 0.0137$, $b = 1.80 \times 10^6$, $c = -3.82 \times 10^{-3}$, and $d = 1.02 \times 10^{-5}$ in the appropriate units. In Fig. 2 the specific heat capacity curve for the supercooled liquid is extrapolated down to the Kauzmann temperature, T_K, which is widely considered to be the lower bound for the glass transition for thermodynamic reasons. The Kauzmann temperature T_K (or isentropic temperature) is the point at which the entropy of the undercooled liquid reaches the entropy of the crystal.[14]

From the measured specific heat capacity data, we can calculate the thermodynamic functions of the $Mg_{65}Cu_{25}Y_{10}$ alloy as a function of temperature. The Gibbs free energy of the undercooled liquid with respect to the crystal, $\Delta G_{l-x}(T)$, can be calculated by integrating the specific heat capacity difference according to the equation

$$\Delta G_{l-x}(T) = \Delta H_f - \Delta S_f \cdot T - \int_T^{T_f} \Delta c_p^{l-x}(T')\,dT' + T \int_T^{T_f} \frac{\Delta c_p^{l-x}(T')}{T'}\,dT', \tag{6}$$

where ΔH_f and ΔS_f are the enthalpy and entropy of fusion, respectively, at the temperature T_f. T_f is the temperature where the Gibbs free energy of the crystal and the liquid are equal. Δc_p^{l-x} is the difference in specific heat capacity between liquid and crystal. Although the T_f is not exactly known for the alloy, from the DSC curve near the melting temperature, we observe that the alloy is virtually at the eutectic composition with a small melting interval. For the calculations we choose the eutectic temperature as T_f.

The calculated entropy of the undercooled $Mg_{65}Cu_{25}Y_{10}$ liquid with respect to the crystal is shown in Fig. 3. The entropy of the undercooled liquid decreases with increasing undercooling until it reaches the entropy of the crystal at the Kauzmann temperature which equals 320 K. The entropy is drawn further below the Kauzmann temperature down to the Vogel–Fulcher–Tammann (VFT) temperature T_0. In this temperature range the entropy of the supercooled liquid would be smaller than that of the crystalline mixture. This means its configurational (communal) entropy would be smaller than that of the crystal.

Figure 4 shows the calculated enthalpy difference between undercooled liquid and the crystalline state. The specific heat capacity is integrated from T_f down to the VFT-temperature T_0. In real experiments residual enthalpy is frozen in as the liquid undergoes the glass transition upon undercooling. Figure 4 shows the approximate residual enthalpy that remains after cooling with the relatively low rate of 0.0167 K/s. By isothermal annealing the alloy can be brought to a lower enthalpic state. This also applies to the entropy that is shown in Fig. 3 where residual entropy is frozen in at the kinetic glass transition.

The calculated Gibbs free energy function with respect to the crystalline state is plotted in Fig. 5. Since the entropy of fusion for this alloy is relatively small, the slope of the Gibbs free energy curve just below the melting point is small which leads to a small driving force for crystallization. The small driving force turns out to be one crucial factor in understanding the high glass forming ability of bulk metallic glass.

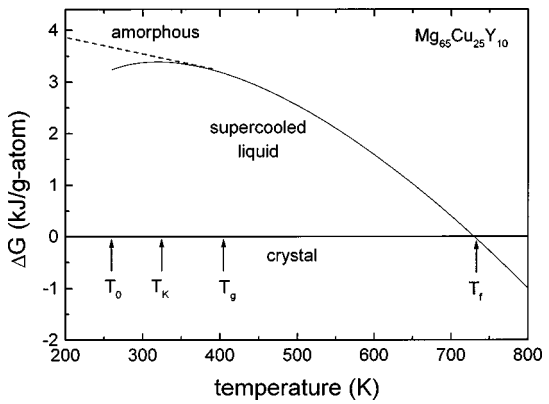

FIG. 5. Gibbs free energy of the undercooled liquid with respect to the crystal as a function of temperature.

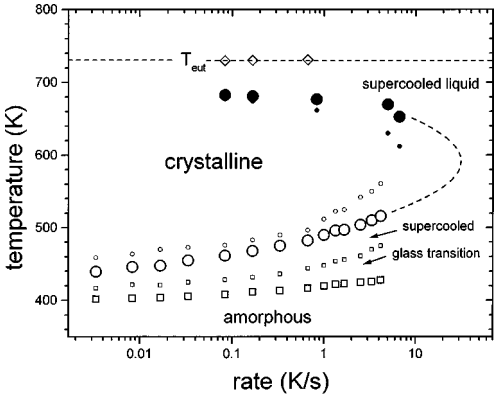

FIG. 6. A temperature-transformation diagram for the $Mg_{65}Cu_{25}Y_{10}$ alloy as a function of heating or cooling rate measured in a DSC. The data for the glass transition upon heating (□), crystallization upon heating (○), and crystallization upon undercooling (●) are shown. Large symbols represent the onset and small symbols the end of the respective transformation. The eutectic reaction upon heating (◇) is independent of the heating rate.

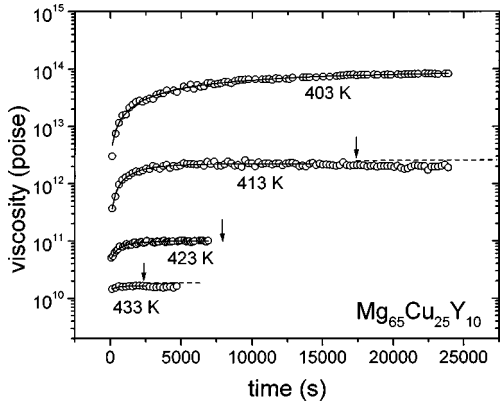

FIG. 7. Isothermal viscosity measurements in the glass transition region by three-point beam bending. The curves are fitted with Eq. (7) in the time range before crystallization (marked by arrows) sets in. The onset times for crystallization were determined independently by isothermal DSC experiments.

B. Kinetics

The transformations from the amorphous into the supercooled liquid state as well as the crystallization from the supercooled liquid state into the crystalline phases were investigated in the DSC with different heating and cooling rates. Figure 6 summarizes the data obtained on the onsets (large symbols) and end points (small symbols) of the glass transition (□) as well as crystallization on heating (○) and undercooling (●) below the eutectic temperature. These transformations are all a function of the rate, whereas the onset of melting (◇) upon heating is independent of the rate since overheating effects are not observable on the time scale of the experiments. The crystallization data from the supercooled liquid state lead to the typical ''nose'' shape. Even though we could not bypass the nose in the DSC due to its limited heating and cooling capacity we can estimate the critical cooling rate to be of the order of 50 K/s. The heating rate dependence of the glass transition is related to the temperature dependence of the structural (α-) relaxation time of the alloy and the temperature dependence of the viscosity.

Viscosities were measured using the beam bending method in a range between 10^8 and 10^{15} poise. In order to obtain equilibrium in the high viscosity regime the samples had to be allowed to relax into their equilibrium state. All samples were heated with the same rate of 0.833 K/s to their annealing temperature and held there until equilibrium was reached. Figure 7 shows isothermal viscosity measurements at different temperatures. The lower the annealing temperature the higher is the equilibrium viscosity and the longer the relaxation time to reach equilibrium. The data were fitted with a stretched exponential relaxation function

$$\eta(t) = \eta_a + \eta_{\text{eq-a}}(1 - e^{-(t/\tau)^{\beta}}) \tag{7}$$

in which τ is an average shear flow relaxation time, β a stretching exponent, t the time, and η_a the viscosity of the amorphous alloy before relaxation. $\eta_{eq\text{-}a}$ is the total viscosity change during relaxation from the amorphous state into the equilibrium state. It was shown earlier that the equilibrium state is equivalent to the supercooled state if observed on a long time scale.[15] Therefore the observed relaxation can be understood as an isothermal glass transition. During isothermal annealing the alloys start to crystallize. Arrows in Fig. 7 mark the onset of primary crystallization as determined in isothermal DSC experiments (not shown). The primary crystallization proceeds by the formation of nanocrystals embedded in a supercooled liquid matrix.[12] A small volume fraction of particles should increase the viscosity slightly according to the Einstein equation.[16] We, however, observe that the viscosity decreases by a small amount upon the formation of crystals. We attribute this to the fact that the remaining matrix changes its composition towards an alloy with a smaller viscosity under isothermal conditions. This is confirmed by the fact that the calorimetric glass transition of the matrix is lowered by about 5 K after the precipitation of nanocrystals, when measured in the DSC with constant heating rate. This means that the relaxation time and thus the viscosity of the matrix at a given temperature are smaller than in the initial alloy. This effect slightly overcompensates the increase of the apparent viscosity due to formation of nanocrystals.

Figure 8 shows the equilibrium viscosity of $Mg_{65}Cu_{25}Y_{10}$ after proper relaxation in an Ahrrenius plot (●). The plot also includes the viscosity data observed in the beginning of the isothermal measurements when the alloy was still in the amorphous state (○). The equilibrium data were fitted by the VFT equation

$$\eta = \eta_0 \cdot \exp\left(\frac{D^* \cdot T_0}{T - T_0}\right). \tag{8}$$

In this formula D^* is the fragility parameter and T_0 is the VFT temperature. The best fit of the experimental data yields $D^* = 22.1$ and $T_0 = 260$ K. The value η_0 was set as 3×10^{-4} P according to the relation $\eta_0 = N_A \cdot h/V$, where, N_A is Avogadro's constant, h is the Planck constant, and V is the molar volume.[17]

At a temperature of 404 K we find a viscosity of 10^{13} P. This temperature corresponds to the onset value of the calorimetric glass transition for a heating rate of 0.0167 K/s.

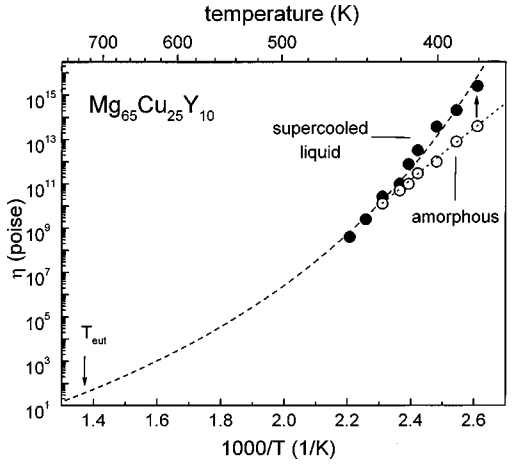

FIG. 8. Measured equilibrium viscosity (●) in an Ahrrenius plot. The data were fitted with the VFT [Eq. (8)] (dashed). Also shown is the viscosity of the amorphous alloy immediately after heating the material to the respective temperature with 0.833 K/s (○). The isothermal relaxation pathway (arrow) is shown in Fig. 7 for selected temperatures.

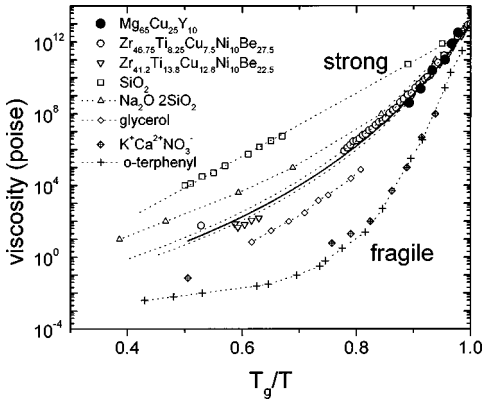

FIG. 10. Fragility plot of the viscosities of $Mg_{65}Cu_{25}Y_{10}$, two Zr–Ti–Cu–Ni–Be bulk metallic glasses (see Ref. 6) and several nonmetallic ''strong'' and ''fragile'' glasses. The data on nonmetallic glasses were taken from Ref. 19.

IV. DISCUSSION

A. Thermodynamics

In this work the thermodynamic functions of the $Mg_{65}Cu_{25}Y_{10}$ alloy were determined as a function of temperature by measuring the heat of fusion as well as the temperature dependence of the specific heat capacity difference between the liquid state and the crystalline state. In Fig. 9, the Gibbs free energy difference between the supercooled liquid and the crystalline mixture is compared with a selection of other eutectic, or close to eutectic, glass forming systems.[18] The alloys show different critical cooling rates between 1 K/s for the pentary $Zr_{41.2}Ti_{13.8}Cu_{12.5}Ni_{10}Be_{22.5}$ and about 10^4 K/s for the binary $Zr_{62}Ni_{38}$. The glass formers with the lower critical cooling rates have smaller Gibbs free energy differences with respect to the crystalline state than the glass formers with high critical cooling rates. Increasing bulk metallic glass forming ability is consistent with a smaller driving force for crystallization. This originates mainly from the smaller entropy of fusion, which determines the slope of the free energy curve at the melting point. The small entropy of these deep eutectic bulk metallic glass forming systems in the melt suggests that they already have a small free volume and a tendency to develop chemical short range order at the melting point. This findings are consistent with the assumption that in multicomponent systems the crystalline phases exhibit relatively large configurational entropies of mixing and with the fact that bulk metallic glass formers are very viscous and relatively dense liquids at the melting point and upon undercooling as will be discussed below.

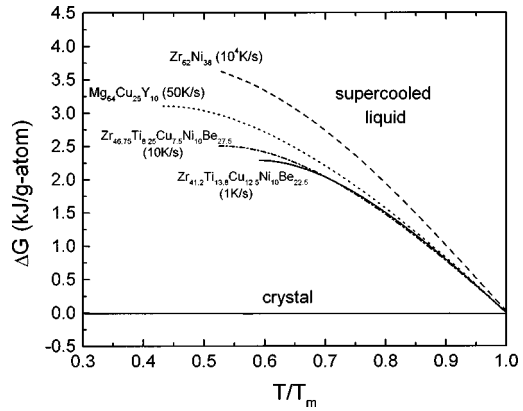

FIG. 9. Gibbs free energy difference between the supercooled liquid and the crystalline mixture for different glass forming alloys (see Ref. 18).

B. Strong liquid behavior

The increasing viscosity of the liquid as a function of temperature reflects the decreasing mobility of atoms upon supercooling. This is observed in all supercooled liquids whether they are metallic or nonmetallic. Silicate liquids usually show high equilibrium melt viscosities and Ahrrenius behavior of the slowdown of mobility in the supercooled melt. They are called strong liquids. The other extreme cases are fragile liquids with low melt viscosities and a more abrupt change of the kinetics close to the glass transition. The fragility concept, proposed by Angell,[19] is a classification scheme to describe the different temperature dependencies of the viscosity. In order to compare the measured viscosities of different glass forming systems the viscosity is normalized to the temperature where the viscosity of the respective alloy is 10^{13} P, which we here refer to as the laboratory glass transition temperature T_g. In the VFT equation [Eq. (8)] the VFT-temperature T_0 is the temperature where the barriers with respect to flow go to infinity and D^* is a measure of the fragility of the liquid. It is found that D^* is of the order of 2 for the most fragile liquids and yields 100 for the strongest glass former SiO_2.

Figure 10 shows the viscosity of the BMG forming $Mg_{65}Cu_{25}Y_{10}$ liquid in comparison with a selection of some nonmetallic liquids as well as two Be-bearing BMG. As mentioned above, strong glass formers, like SiO_2, are one extreme case. They exhibit a very small VFT temperature and a very high melt viscosity. Fragile glass formers show a VFT temperature near the glass transition temperature, as

well as low melt viscosities. The $Mg_{65}Cu_{25}Y_{10}$ and the Zr–Ti–Cu–Ni–Be BMG behave closer to the strong glasses than to the fragile glasses. The melt viscosity of BMGs is of the order of 50 P. They are much more viscous than pure metals or some binary alloys, where viscosities of the order of 5×10^{-2} P are observed. The strong liquid behavior of BMG, as reflected by the temperature dependence of their viscosity, plays an important role in understanding the superior glass forming ability compared to other metallic liquids since the kinetics stay sluggish in the entire supercooled liquid region and leads to a low nucleation and growth rate. This is discussed elsewhere in detail.[6,20]

C. Entropy and viscosity

Adam and Gibbs[21] developed a well-known theory on cooperative relaxation in liquids based on the entropy. In this model the decrease of configurational entropy accounts for the increasing relaxation time and viscosity in the supercooled liquid. The viscosity is expressed as

$$\eta=\eta_0\cdot\exp\left(\frac{C}{T\cdot S_c}\right) \tag{9}$$

in which S_c is the configurational entropy of the liquid and C a constant that represents the free enthalpy barrier to cooperative rearrangements. Assuming that a difference in vibrational entropy between the supercooled liquid and the crystal can be neglected, the configurational entropy is usually approximated by the entropy difference between the supercooled liquid and the crystal ($S_c\approx\Delta S$). The configurational entropy of the liquid at the melting point is set equal to the entropy of fusion. We can apply this equation to our viscosity data, since we know the functional form of the entropy difference. It is commonly assumed that the configurational entropy vanishes at the Kauzmann temperature and therefore the viscosity diverges at the Kauzmann point.

However, in a multicomponent system the crystal can also have considerable configuration entropy resulting from the entropy of mixing. In fact, a disordered solid solution or an intermetallic compound with extended solubility might even have a larger entropy of mixing than a deeply undercooled liquid with small free volume and a strong tendency to develop chemical and topological short-range order. We therefore do not assume that the Kauzmann temperature is necessarily the temperature where the configurational entropy of the liquid goes to zero. We use a configurational entropy of the form

$$S_c(T)=S_c^m-\int_T^{T_m}\Delta c_p\,dT' \tag{10}$$

in which we use the configurational entropy, S_c^m, at the melting point is a parameter to fit the viscosity data according to Eq. (9). The prefactor η_0 in Eq. (9) is chosen the same way as in the VFT fit, addressing the experimental finding that the extrapolations of all viscosity curves for different materials meet at infinite temperature in the fragility plot (see Fig. 10).

Figure 11 shows the results of the analysis. The viscosity data cannot be fitted with a S_c^m that equals the entropy of fusion and a S_c that vanishes at the Kauzmann temperature.

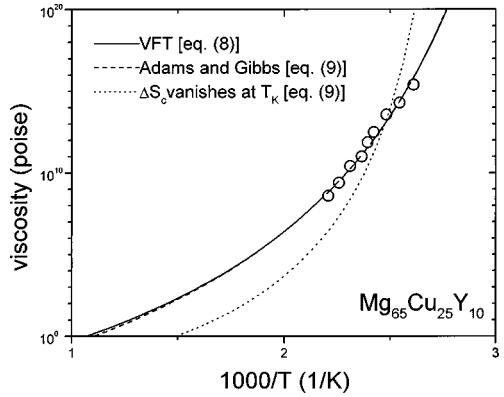

FIG. 11. Comparison of the VFT fit (solid) and two fits according to the Adam–Gibbs theory. The experimental viscosity data (○) cannot be fitted with Eq. (9) (dotted) under the assumption that the configurational entropy of the liquid vanishes at the Kauzmann temperature. If we assume that the configurational entropy of the supercooled liquid becomes smaller than that of the crystalline mixture and vanishes at about T_0, the fit to Eq. (9) is in excellent agreement with the VFT fit [Eq. (8)].

However, VFT fit and Adam–Gibbs fit are in excellent agreement, if the configurational entropy difference at the melting point is set to be 16.8 J/g atom K instead of the entropy of fusion which amounts to 11.8 J/g atom K (see also Fig 3). S_c of the liquid vanishes at 270 K close to the VFT temperature. In this picture the supercooled liquid can exist below the Kauzmann temperature. After sufficiently long relaxation the entropy of the supercooled liquid would become smaller than that of the crystal. The case of a supercooled liquid having a lower entropy than a crystal was observed previously during ''inverse melting'' in Cr–Ti and similar systems.[22,23] In these cases the crystalline phase was a metastable bcc solid solution.

A relaxation from the amorphous state into a supercooled liquid state at the Kauzmann temperature is experimentally not attainable. From the viscosity data we estimate that the relaxation time at 320 K would be more than 10^{25} s (3×10^{17} years). Complete crystallization at that temperature will occur much earlier after 300 000 years.

It is worth noting that the fragility and the specific heat capacity of the liquid are in general at least qualitatively connected. Strong glass formers show small Δc_p upon supercooling, whereas fragile glass formers exhibit rapidly increasing specific heat capacities, especially when approaching the glass transition. In a special case, the viscosity and Δc_p are quantitatively connected. If $\Delta c_p\propto1/T$, Eq. (9) is equivalent to the VFT Eq. (8) (see, e.g., Ref. 24). In the case of the $Mg_{65}Cu_{25}Y_{10}$ alloy the Δc_p can be approximated well with this hyperbolic temperature dependence. Therefore the VFT fit and the Adam–Gibbs fit are in such a good agreement (Fig. 11). But this is only the case if we are assuming that the configurational entropy vanishes close to the VFT temperature and not at the isentropic temperature.

D. Glass transition and viscosity

We finally want to compare the kinetics of the glass transition with the measured viscosity. As shown in Fig. 6, the temperature range in which the glass transition occurs is a function of heating rate. Since the glass transition repre-

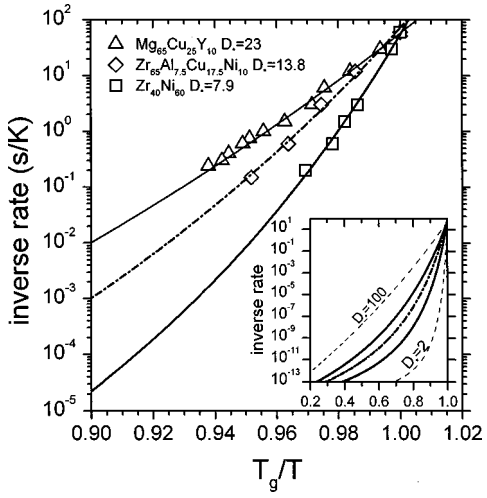

FIG. 12. Inverse heating rate as a function of onset temperature for the glass transition normalized to the onset temperature of the glass transition measured with a rate of 0.0167 K/min. The data were fitted with Eq. (11). The fragility parameter D^* for the $Mg_{65}Cu_{25}Y_{10}$ alloy is in very good agreement with the value found by fitting the viscosity data to the VFT [Eq. (8)].

sents the relaxation from the amorphous state into the supercooled liquid state, the heating rate dependence should be a measure for this relaxation. The inverse heating rate should be approximately proportional to the structural (α-) relaxation time.

In Fig. 12 the inverse heating rate is plotted as a function of onset temperature of the glass transition. The data are fitted with the VFT-type equation

$$\tau = \tau_0 \cdot \exp\left(\frac{D^* \cdot T_0}{T - T_0}\right) \tag{11}$$

in which τ is the inverse heating rate and T the onset of the glass transition. Figure 12 shows the result for the $Mg_{65}Cu_{25}Y_{10}$ alloy as well as the results for two other glass forming alloys. The resulting fragility parameters are indicated in the plot. For the $Mg_{65}Cu_{25}Y_{10}$ we find a very good agreement with the D^* obtained from the fit to the viscosity data. This suggests that the heating rate dependence of the kinetic glass transition is a measure for the fragility of the glass. A small heating rate dependence indicates a fragile glass, whereas a large heating rate dependence is characteristic for a strong glass.

The data on the other two glass forming systems depicted in the plot suggest that they are more fragile glass formers. The ''conventional'' $Zr_{40}Ni_{60}$ metallic glass is the most fragile of the alloys investigated. It is interesting to note that previous metallic glass formers in general showed small heating rate dependencies of the glass transition indicating that they are fragile glasses.

V. SUMMARY AND CONCLUSION

The thermodynamics and kinetics of the $Mg_{65}Cu_{25}Y_{10}$ alloy were studied in the supercooled liquid state and at the glass transition. Absolute values of c_p were measured with respect to sapphire standards for amorphous alloy, crystal, supercooled liquid, and melt. The specific heat capacity of the liquid is a decreasing function with temperature. Entropy, enthalpy, and Gibbs free energy difference between supercooled liquid and crystal as a function of temperature were calculated. The calculations show that the Gibbs free energy difference between liquid and solid state stays relatively small upon undercooling. This originates mainly from the relatively small entropy of fusion of the alloy. The relatively small Gibbs free energy difference appears to be a contributing factor in the high glass forming ability of the alloy.

The viscosities of the amorphous alloy throughout the glass transition into the supercooled liquid region were measured using the three-point beam bending method. The measured viscosities ranged from 10^8 to 10^{15} P. The Vogel–Fulcher–Tammann fit to the data shows that the alloy is a relatively strong liquid similar to Zr–Ti–Cu–Ni–Be bulk metallic glass forming liquids. Both the small driving force for nucleation and the sluggish kinetics in the supercooled liquid substantially retard the nucleation of crystals from a homogeneous liquid.

The comparison between the VFT fits to the data and the Adam–Gibbs approach based on the change of configurational entropy suggests that the configurational entropy of the supercooled liquid in principle can become smaller than that of the crystal. However, in the respective temperature range the crystallization would precede relaxation into the supercooled liquid state.

The strong liquid nature of the $Mg_{65}Cu_{25}Y_{10}$ alloy is revealed by (1) the temperature dependence of the viscosity, (2) the relatively small specific heat capacity difference between liquid and crystal, especially close to the glass transition, and (3) the pronounced heating rate dependence of the glass transition.

ACKNOWLEDGMENTS

This work was supported by the U.S. Department of Energy (Grant No. DEFG-03-86ER45242). Partial support for R. Busch was provided by the Alexander von Humboldt Foundation via the Feodor Lynen Program.

[1] A. Inoue, T. Zhang, and T. Masumoto, Mater. Trans., JIM **31**, 425 (1991).
[2] T. Zhang, A. Inoue, and T. Masumoto, Mater. Trans., JIM **32**, 1005 (1991).
[3] A. Inoue, A. Kato, T. Zhang, S. G. Kim, and T. Masumoto, Mater. Trans., JIM **32**, 609 (1991).
[4] A. Peker and W. L. Johnson, Appl. Phys. Lett. **63**, 2342 (1993).
[5] R. Busch, Y. J. Kim, and W. L. Johnson, J. Appl. Phys. **77**, 4039 (1995).
[6] R. Busch, A. Masuhr, E. Bakke, and W. L. Johnson, Mater. Res. Soc. Symp. Proc. **455**, 369 (1997).
[7] U. Geyer, S. Schneider, W. L. Johnson, Y. Qiu, T. A. Tombrello, and M. P. Macht, Phys. Rev. Lett. **75**, 2364 (1995).
[8] R. Busch, Y. J. Kim, W. L. Johnson, A. J. Rulison, W. K. Rhim, and D. Isheim, Appl. Phys. Lett. **66**, 3111 (1995).
[9] H. E. Hagy, J. Am. Ceram. Soc. **46**, 93 (1963).
[10] F. T. Trouton, Proc. R. Soc. London **77**, 426 (1906).
[11] M. Reiner, in *Rheology*, edited by F. R. Eirich (Academic, New York, 1956), Vol. 1, p. 9.
[12] W. Liu, Ph.D. thesis, California Institute of Technology, 1997.
[13] O. Kubaschewski, C. B. Alcock, and P. J. Spencer, *Materials Thermochemistry*, 6th ed. (Pergamon, New York, 1993).
[14] W. Kauzmann, Chem. Rev. **43**, 219 (1948).
[15] R. Busch and W. L. Johnson, Appl. Phys. Lett. (in press).
[16] A. Einstein, Ann. Phys. (Leipzig) **34**, 592 (1911).

[17] S. V. Nemilov, Glass Phys. Chem. **21**, 91 (1995).
[18] R. Busch, E. Bakke, and W. L. Johnson, Mater. Sci. Forum **235–238**, 327 (1996).
[19] C. A. Angell, Science **267**, 1924 (1995).
[20] R. Busch, A. Masuhr, E. Bakke, and W. L. Johnson, Mater. Sci. Forum (in press).
[21] G. Adam and J. H. Gibbs, J. Chem. Phys. **43**, 139 (1965).
[22] H. Z. Yan, T. Klassen, C. Michaelsen, M. Oehring, and R. Bormann, Phys. Rev. B **47**, 8520 (1993).
[23] C. Michaelsen, W. Sinkler, T. Pfullmann, and R. Bormann, J. Appl. Phys. **80**, 2156 (1996).
[24] C. A. Angell, J. Non-Cryst. Solids **131–133**, 13 (1991).